NUCL SCI TECH (2019) 30:89
https://doi.org/10.1007/s41365-019-0615-1

Hydrodynamic characteristics of 30%TBP/kerosene-HNO_3 solution system in an annular centrifugal contactor

Hong-Lin Chen[1] · Jian-Chen Wang[1] · Wu-Hua Duan[1,2] · Jing Chen[1,2]

Received: 28 September 2018 / Revised: 19 November 2018 / Accepted: 23 February 2019 / Published online: 14 May 2019

Abstract Annular centrifugal contactors (ACCs) have many advantages and are recognized as key solvent-extraction equipment for the future reprocessing of spent nuclear fuel (RSNF). To successfully design and operate ACCs for RSNF, it is necessary to understand the hydrodynamic characteristics of the extraction systems in ACCs. The phase ratio ($R = V_{aq}/V_{org}$, A/O) and liquid holdup volume (V) of the ACC are important hydrodynamic characteristics. In this study, a liquid-fast-separation method was used to systematically investigate the effects of the operational and structural parameters on the V and R (A/O) of a ϕ20 ACC by using a 30%TBP/kerosene-HNO_3 solution system. The results showed that the operational and structural parameters had different effects on the V and R (A/O) of the mixing and separating zones of the ACC, respectively. For the most frequently used structural parameters of the ϕ20 ACC, when the rotor speed was 3500 r/min, the total flow rate was 2.0 L/h, and the flow ratio (A/O) was 1, the liquid holdup volumes in the mixing zone and rotor were 8.03 and 14.0 mL, respectively, and the phase ratios (A/O) of the mixing zone and separating zone were 0.96 and 1.43, respectively.

Keywords Annular centrifugal contactor · Liquid-fast-separation method · Phase ratio (A/O) · Liquid holdup volume · Structural parameter · Operational parameter

1 Introduction

Reprocessing of spent nuclear fuel (RSNF) can recover nuclear resources and reduce nuclear waste and is thus a crucial part of an advanced nuclear fuel cycle for ensuring the sustainable development of nuclear energy. Currently, the plutonium uranium recovery by extraction (PUREX) process employing tri-*n*-butyl phosphate (TBP) as the extractant and *n*-dodecane or kerosene as the diluent is the only commercial reprocessing process in the world [1].

An annular centrifugal contactor (ACC) separates the dispersion of two phases by using centrifugal force [2]. As shown in Fig. 1, two immiscible liquids in the annular zone are initially mixed intensively by the spinning rotor to form the dispersion. The dispersion then flows into the separating zone of the rotor through the rotor inlet and is separated rapidly owing to the centrifugal force induced by the spinning rotor. After separation, the two phases finally flow through their respective weirs and collectors into their respective collection tanks or adjacent stages.

ACCs offer many advantages, including a short residence time and low solvent degradation by irradiation because of their small liquid holdup volume (V), high compactness, high nuclear criticality safety, high mass-transfer efficiency, excellent phase separation, and easy operation [3, 4]. ACCs have been utilized successfully in

This work was supported by the Program for Changjiang Scholars and Innovative Research Team in University of Ministry of Education of China (No. IRT13026) and the National 863 Program for Nuclear Fuel Cycling and Nuclear Safety Technology Project (No. 2009AA050703).

✉ Wu-Hua Duan
dwh203@mail.tsinghua.edu.cn

[1] Institute of Nuclear and New Energy Technology, Collaborative Innovation Center of Advanced Nuclear Energy Technology, Tsinghua University, Beijing 100084, China

[2] Beijing Key Lab of Radioactive Waste Treatment, Tsinghua University, Beijing 100084, China

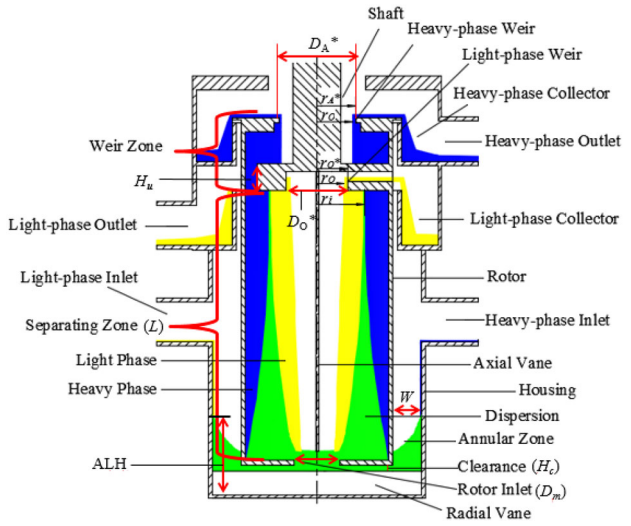

Fig. 1 (Color online) Schematic of the ACC

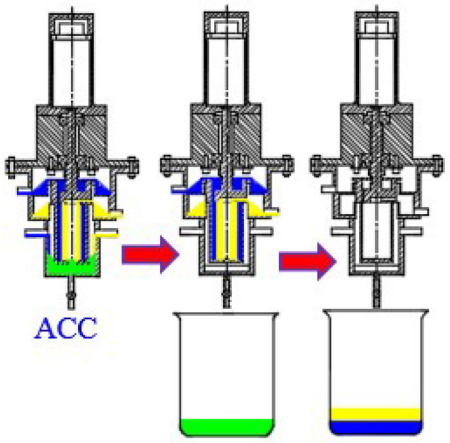

Fig. 2 (Color online) Liquid discharging method

various demonstration tests of many solvent-extraction processes for RSNF and the partitioning of high-level liquid waste [5–14]. Moreover, ACCs are recognized as key solvent-extraction equipment for future nuclear fuel-cycle processes. Hence, many countries engaging in RSNF are investigating ACCs [4, 5, 15–17].

The flow in the ACC is three-dimensional, turbulent, transient, and multiphase [18, 19]. Hence, it is difficult to determine the effects of the physical properties, operational parameters, and structural parameters on the hydrodynamic characteristics. The current development of the ACC is recognized as "an art." [20] To successfully design and operate ACCs for RSNF, detailed hydrodynamic characteristic information, including the phase ratio ($R = V_{aq}/V_{org}$, A/O) and liquid holdup volume (V), is required. The R (A/O) and V depend on the operational parameters, structural parameters, and physical properties of the two phases.

However, accurately measuring the V of the ACC and obtaining R (A/O) are difficult because of the unique structure and flow characteristics of the ACC. Zhao used a liquid discharging method to measure the V of a ϕ20 ACC by using a kerosene–water system and then to calculate the interface radius (r_i) of the separating zone and the holdup volume of the mixing zone [21]. The measurement procedures of this method are shown in Fig. 2. Schuur et al. [22] and Ayyappa et al. [23] measured the V of a ϕ50 ACC using the same method. However, the liquid discharging method has the following disadvantages. (1) It requires time to discharge the liquids in the mixing zone completely; hence, some liquids in the mixing zone still flow into the rotor. (2) Some liquids in the rotor are thrown into the collectors during liquid discharging. (3) Some liquids cannot be discharged, because they adhere to the inner wall of the housing. Duan and Cao [24] developed a liquid-fast-separation method based on an advanced self-made ϕ20 ACC to measure the liquid holdup volume. The measurement procedures of this method are shown in Fig. 3.

In this study, the dimensionless dispersion number (N_{Di}) of the 30%TBP/kerosene-HNO_3 solution system was initially determined to evaluate the phase-separation performance of this extraction system. Then, the effects of the operational and structural parameters on the V and R (A/O) of a ϕ20 ACC were systematically investigated using the liquid-fast-separation method and the 30%TBP/kerosene-HNO_3 solution system.

2 Experiments

2.1 Chemicals

TBP (> 98% pure), HNO_3 (analytical purity), and NaOH (analytical purity) were obtained from Beijing Chemical Plant, China. Saturated hydrogenated kerosene

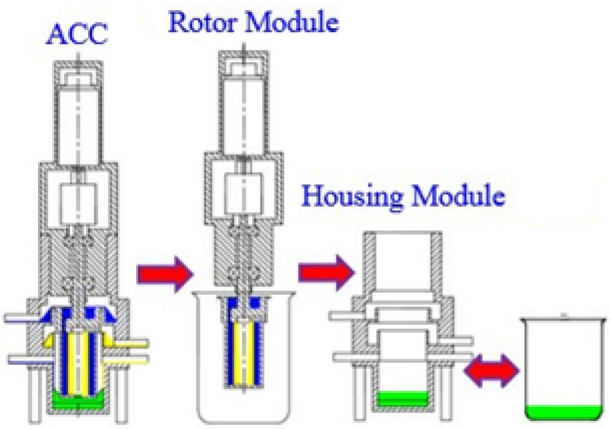

Fig. 3 (Color online) Liquid-fast-separation method

was obtained from Jinzhou Refinery Factory, China. The surface tension, density, and viscosity of the TBP were 27.79 mN/m, 973 kg/m^3, and 3.32 mPa s, respectively. The TBP was diluted using kerosene to 30% TBP/kerosene (v/v) without further purification.

2.2 ϕ20 ACC

The ϕ20 ACC was a self-made solvent-extraction instrument with a rotor inner diameter of 20 mm. It contained two modules—rotor and housing—as shown in Fig. 3 [25]. The rotor module could be easily lifted up and down by a manipulator or by hand because no screw or nut was used to set the two modules. Therefore, the liquid-fast-separation method could be easily performed using this ACC.

2.3 Determination of dispersion number

Leonard proposed the concept of a dimensionless dispersion number (N_{Di}) for evaluating the phase-separation performance of an extraction system. Additionally, he developed a standard test for determining N_{Di} [26]. After N_{Di} is determined, the phase-separation performance of the extraction system can be assessed by referring to Table 1. In this study, the N_{Di} of the 30%TBP/kerosene-HNO_3 solution system was determined according to the standard test.

The test for determining N_{Di} was conducted at room temperature (23 ± 2 °C) using the 30%TBP/kerosene-HNO_3 solution system. First, two immiscible phases of 50 mL each were placed into a 100-mL graduated glass cylinder with a ground-glass stopper. Then, the total height (Δz) of the fluid was measured, and the position of the interface between the two phases was marked. Next, after the graduated cylinder was sealed with the glass stopper, it was shaken vigorously by hand for 20 s, allowed to settle for 10 s and shaken vigorously again for 20 s. Subsequently, the cylinder was immediately placed on a benchtop, and a stopwatch was used to record the time taken for the dispersion band to break. Finally, after the last droplet disappeared and a clear phase interface appeared, the timer was stopped, and the time was recorded. The experiment was repeated thrice, and the average result was calculated to obtain the phase-separation time (t_B). N_{Di} is expressed as follows:

$$N_{Di} = \frac{1}{t_B}\sqrt{\frac{\Delta z}{g}}, \quad (1)$$

where Δz is the total height of the fluid (m), t_B is the time taken for the dispersion band to break (s), and g is the gravitational acceleration (9.8 m/s^2) [26].

Table 1 Criteria for the phase-separation performance rating of an extraction system using N_{Di} [26]

N_{Di}	Phase-separation performance
$\leq 2 \times 10^{-4}$	Unacceptable
2×10^{-4}–4×10^{-4}	Poor
4×10^{-4}–8×10^{-4}	Fair
8×10^{-4}–16×10^{-4}	Good
$\geq 16 \times 10^{-4}$	Excellent

2.4 Determination of liquid holdup volume and phase ratio

Figure 4 shows the experimental system. A regular direct-current (DC) power supply was used to control the rotor speed. Two peristaltic pumps were used to feed the two phases into the ϕ20 ACC.

The rotor included the separating and weir zones, and the mixing zone was composed of the zone under the rotor and the annular zone between the outer wall of the rotor and the inner wall of the housing. The liquid-fast-separation method was used to measure the liquid holdup volumes of the mixing and separating zones. First, the pumps were shut down when the operation of the ACC reached a steady state. Then, the rotor module was manually lifted up and simultaneously moved above a beaker within 2 s. Next, the rotor operation was stopped, and the liquids of the rotor flowed into the beaker and were then transferred into a measuring cylinder. Thus, the liquid holdup volume of the rotor (V_r) was determined. Finally, the liquids in the mixing zone were transferred into a measuring cylinder through a pipette. Hence, the liquid holdup volume of the mixing zone (V_m) was determined. The sum of the two

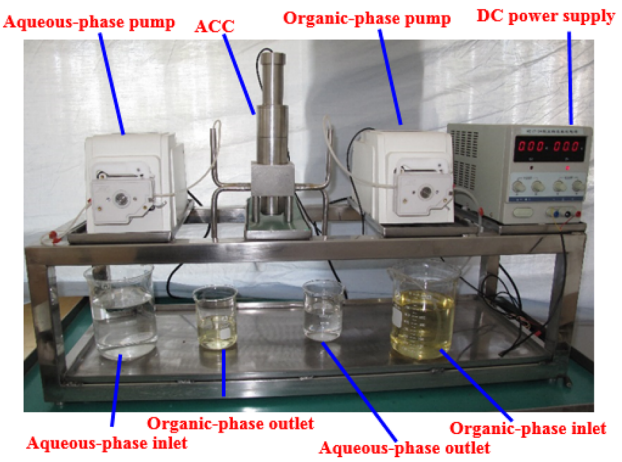

Fig. 4 Experimental system

liquid holdup volumes was the total liquid holdup volume (V_t) of the ACC.

The volume of each phase was determined after the separation of the two phases in each measuring cylinder. Thus, the phase ratios (A/O) in the separating and mixing zones were obtained. The liquid holdup volume of the separating zone (V_s) was obtained as follows:

$$V_s = V_r - V_w, \quad (2)$$

where V_s is the liquid holdup volume of the separating zone (mL), V_r is the liquid holdup volume of the rotor (mL), and V_w is the liquid holdup volume of the weir zone (mL).

In this study, the organic phase was 30%TBP/kerosene, and the heavy phase was an HNO_3 solution. The effects of the operational and structural parameters shown in Table 2 on V and R (A/O) were investigated. When to investigate the effect of one parameter on the V and R (A/O), the values of the other parameters are bold in Table 2. In each experiment, $< 0.5\%$ of the other phase entrainment in either out effluent was required.

3 Results and discussion

3.1 Dispersion number N_{Di}

Figure 5 shows the effects of the HNO_3 concentrations on the N_{Di} of the 30%TBP/kerosene-HNO_3 solution system. As shown, the N_{Di} increased with the HNO_3 concentrations and was $> 14 \times 10^{-4}$ when the HNO_3 concentration was > 0 mol/L. According to Table 1, good phase-separation performance of an extraction system in the ACC is expected when $N_{Di} > 8 \times 10^{-4}$. Hence, the 30%TBP/kerosene-HNO_3 solution system was expected to exhibit good phase-separation performance in the ACC.

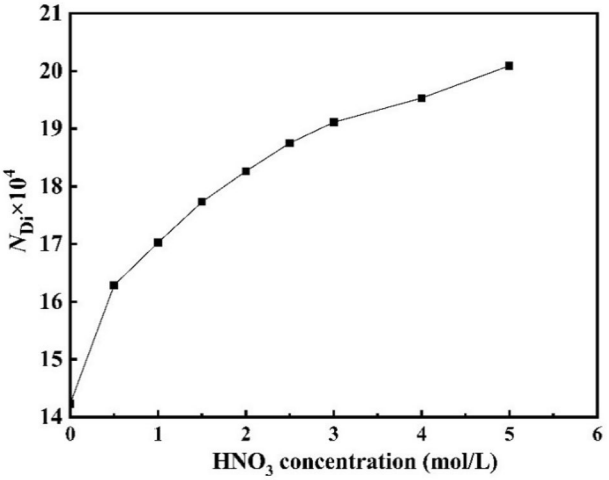

Fig. 5 Effect of the HNO_3 concentration on the N_{Di} of the TBP/kerosene-HNO_3 solution system

3.2 Liquid holdup volume

3.2.1 Effects of operational parameters

Figure 6 shows the effects of the operational parameters, such as the flow ratio (F, A/O), total flow rate of the two phases (Q), and rotor speed (ω), on the liquid holdup volume (V). The liquid holdup volume of the rotor (V_r, approximately 14.0 mL) hardly changed with respect to F (A/O), Q, and ω. The liquid holdup volume of the mixing zone (V_m) initially increased with the increase in F (A/O) and Q and then remained almost constant; however, with the increase in ω, it initially decreased and then remained almost constant. Thus, the effects of the operational parameters on the total liquid holdup volume (V_t) and V_m were identical. When the ACC is operated, the relative pressure at the rotor inlet becomes slightly negative

Table 2 Operational and structural parameters

Parameter types	Parameters	Values				
Operational parameters	Rotor speed (ω, r/min)	3000	**3500**	4000	4500	5000
	Total flow rate (Q, L/h)	0.5	1.0	**2.0**	4.0	6.0
	Flow ratio (F, A/O)	0.25	0.5	**1**	2	4
Structural parameters of housing	Width of annular (W, mm)	2.5	3.5	**4.0**	4.5	5.5
	Number of radial vanes (N_r)	0	2	**4**	6	8
	Height of clearance (H_c, mm)	2.0	3.0	**3.5**	4.0	5.0
Structural parameters of rotor	Length of separating zone (L, mm)	30.0	40.0	**45.0**	50.0	60.0
	Diameter of heavy-phase weir (D_A*, mm)	10.0	10.5	**11.0**	11.5	12.0
	Diameter of light-phase weir (D_O*, mm)	6	7	**8**	9	10
	Height of underflow (H_u, mm)	1	3	**5**	7	9
	Diameter of rotor inlet (D_m, mm)	3	4	**5**	6	7
	Number of axial vanes (N_a)	0	2	**4**		

The bold values are the commonly used parameters of ACCs

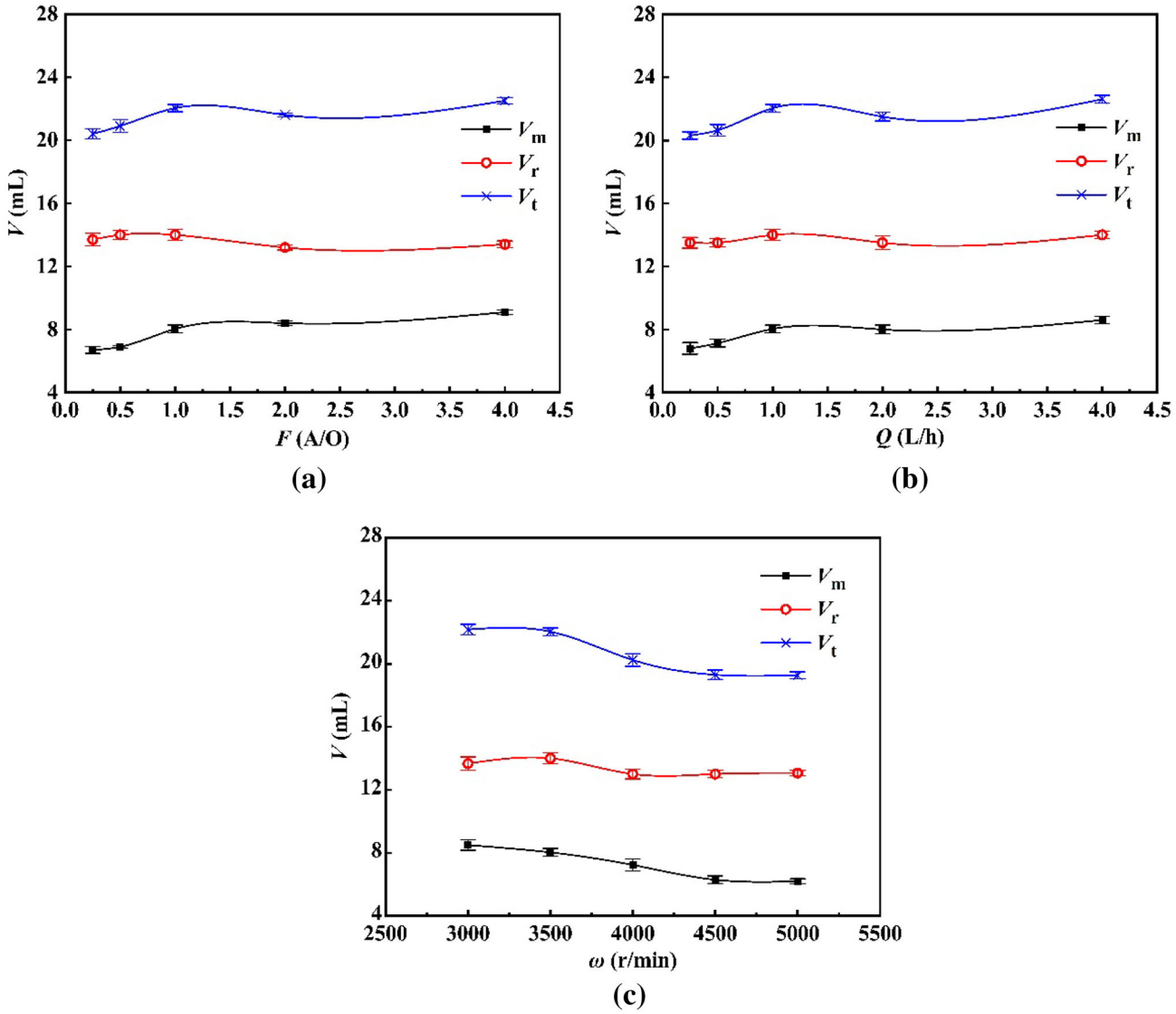

Fig. 6 Effects of the operational parameters on V

[19, 27]. Moreover, a higher ω yields a greater absolute value of the negative pressure. To maintain the balance of the pressure, the annular liquid height (ALH) is decreased with the increase in ω. Hence, V_m is also decreased with the increase in ω. Wardle investigated the effects of F (A/O) and Q on the ALH and reported that the ALH increased with an increase in Q and a decrease in F (A/O) [18]. Our results for the effect of Q agree with those of Wardle. However, our results for the effect of F (A/O) disagree with those of Wardle. All our results for the effects of the operational parameters on V agree with those of Zhao [21] and Duan and Cao [24].

3.2.2 *Effects of structural parameters of housing*

Figure 7 shows the effects of the structural parameters of the housing, including the height of the clearance (H_c), width of the annular (W), and number of radial vanes (N_r), on V. The structural parameters of the housing had almost no effect on V_r, because they hardly influenced the geometric volume of the rotor. V_m increased with H_c and W but decreased with the increase in N_r. Thus, the effects of the structural parameters of the housing on V_t and V_m were the same. When H_c and W increased, the geometric volume of the mixing zone obviously increased; hence, V_m increased. Wardle investigated the effects of N_r on the ALH and reported that with the increase in N_r, the ALH decreased, resulting in the decrease in V_m [18]. Therefore, our results for the effect of N_r on V_m agree with those of Wardle. We

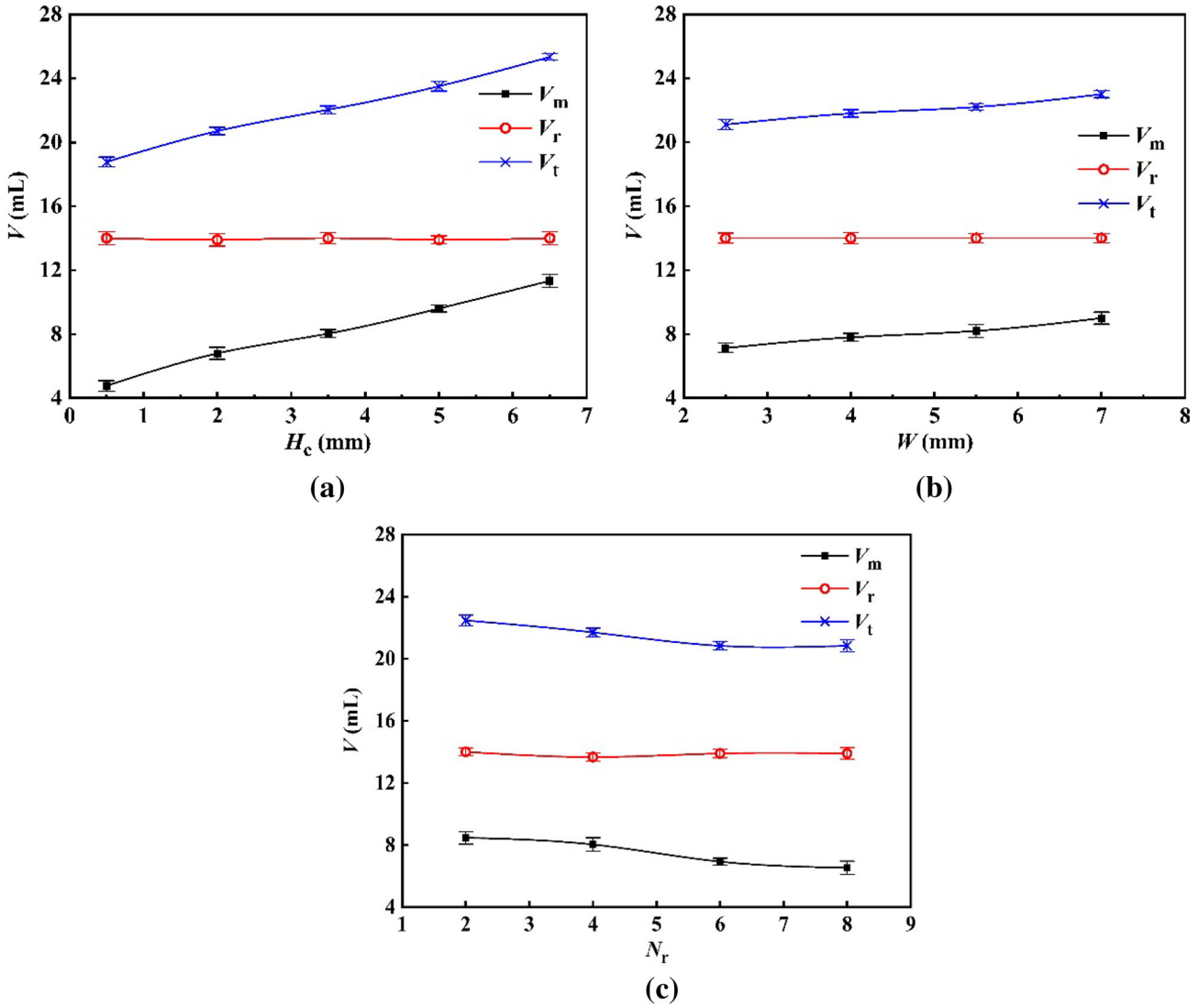

Fig. 7 Effects of the structural parameters of the housing on V

also performed the experiment without radial vanes, i.e., with $N_r = 0$. The results showed that the ACC could not operate normally without radial vanes, because the liquids in the mixing zone could not be absorbed into the rotor.

3.2.3 Effects of structural parameters of rotor

Figure 8 shows the effects of the structural parameters of the rotor, including the diameter of the heavy-phase weir (D_A*), diameter of the light-phase weir (D_O*), length of the separating zone (L), height of the underflow (H_u), and diameter of the rotor inlet (D_i), on V. V_r hardly changed (approximately 14.0 mL) with respect to D_A* and H_u but increased with L and decreased with the increase in D_O*. The structural parameters of the rotor had almost no effect on V_m, because they hardly influenced the geometric volume and flow of the mixing zone. Accordingly, the effects of the structural parameters of the rotor on V_t and V_r were the same. In the ϕ20 ACC, when D_A* was 12 mm, an organic-phase entrainment occurred in the aqueous-phase outlet under the experimental conditions. Variations in D_A*, H_u, and D_i hardly affected the geometric volume of the rotor, thus hardly influencing V_r. The geometric volume of the separating zone increased with the increase in L and the decrease in D_O*.

Table 3 shows the effects of the number of axial vanes (N_a) on V for the ACC. N_a hardly affected V_m, because it hardly influenced the geometric volume and flow of the mixing zone. V_r increased slightly with the increase in N_a. Accordingly, the V_t of the ϕ20 ACC increased slightly with the increase in N_a The axial vanes were used to accelerate the dispersion in the separating zone to ω. During the experiment, when the rotor module was lifted, some liquids in the separating zone flowed into the mixing zone.

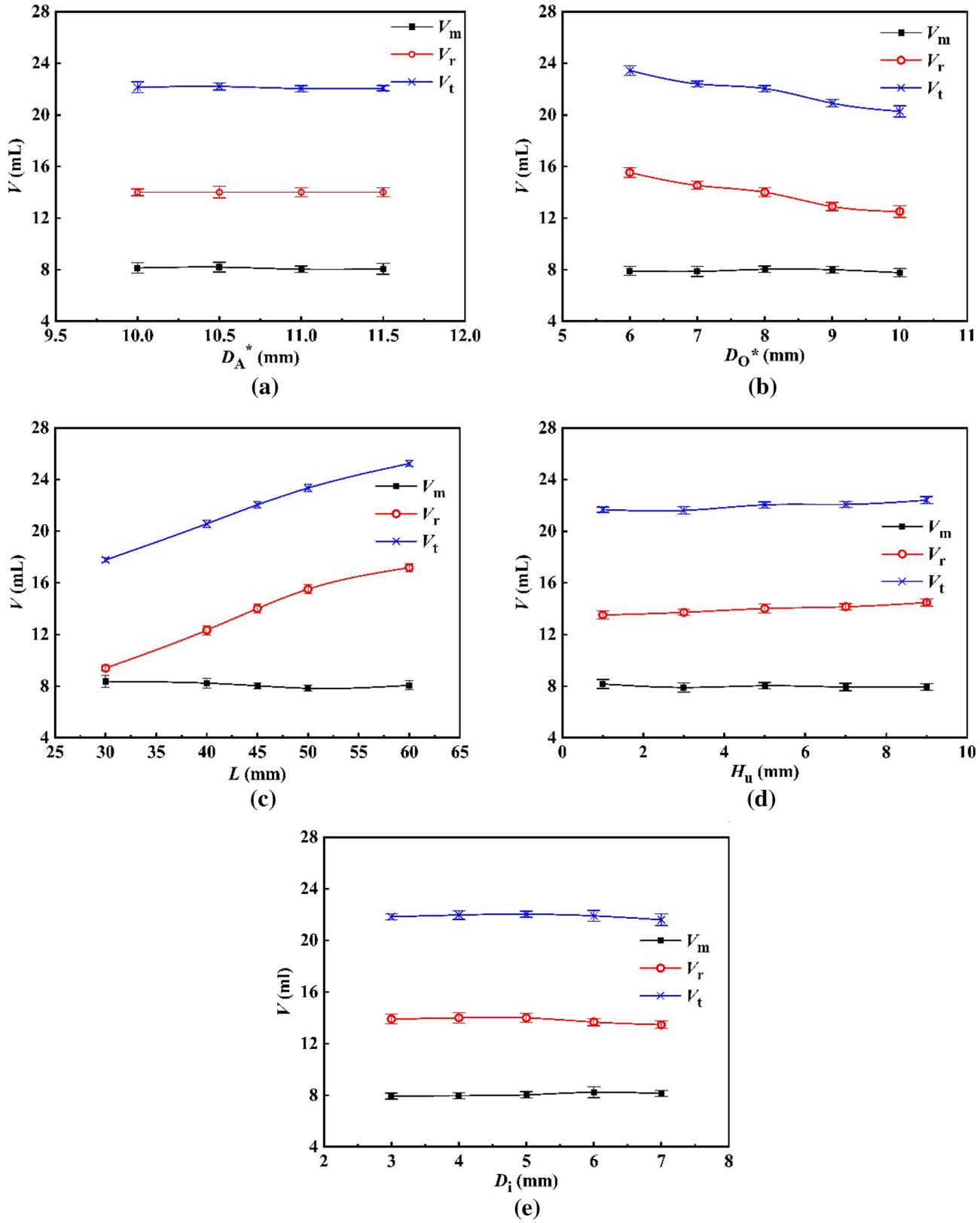

Fig. 8 Effects of the structural parameters of the rotor on V

Table 3 Effects of N_a on V and R (A/O)

N_a	V_m (mL)	V_r (mL)	V_t (mL)	R_m (A/O)	R_s (A/O)
0	8.25	12.75	21.0	0.92	2.19
2	7.97	13.4	21.37	0.99	1.71
4	8.03	14.0	22.03	0.96	1.43

Reducing the rotation speed of the liquids in the separating zone caused the liquids to flow out easily. Therefore, the number of axial vanes had almost no effect on V_m and V_r during the operation of the ϕ20 ACC.

3.3 Phase ratio (A/O)

3.3.1 Effects of operational parameters

Figure 9 shows the effects of the operational parameters—F (A/O), Q, and ω—on R (A/O). The phase ratio of the mixing zone (R_m, A/O) decreased with the increase in Q and increased with the increase in ω and F (A/O). The phase ratio of the separating zone (R_s, A/O) decreased with the increase in ω and increased with the increase in Q and F (A/O). When ω was 3500–4000 r/min, R_m (A/O) was close to F (A/O). However, when Q was large or ω was low, R_m (A/O) was lower than F (A/O). When Q was small or ω was high, R_m (A/O) was higher than F (A/O). The density of the aqueous phase (ρ_A) was higher than that of the organic phase; thus, the upper and lower sections of the

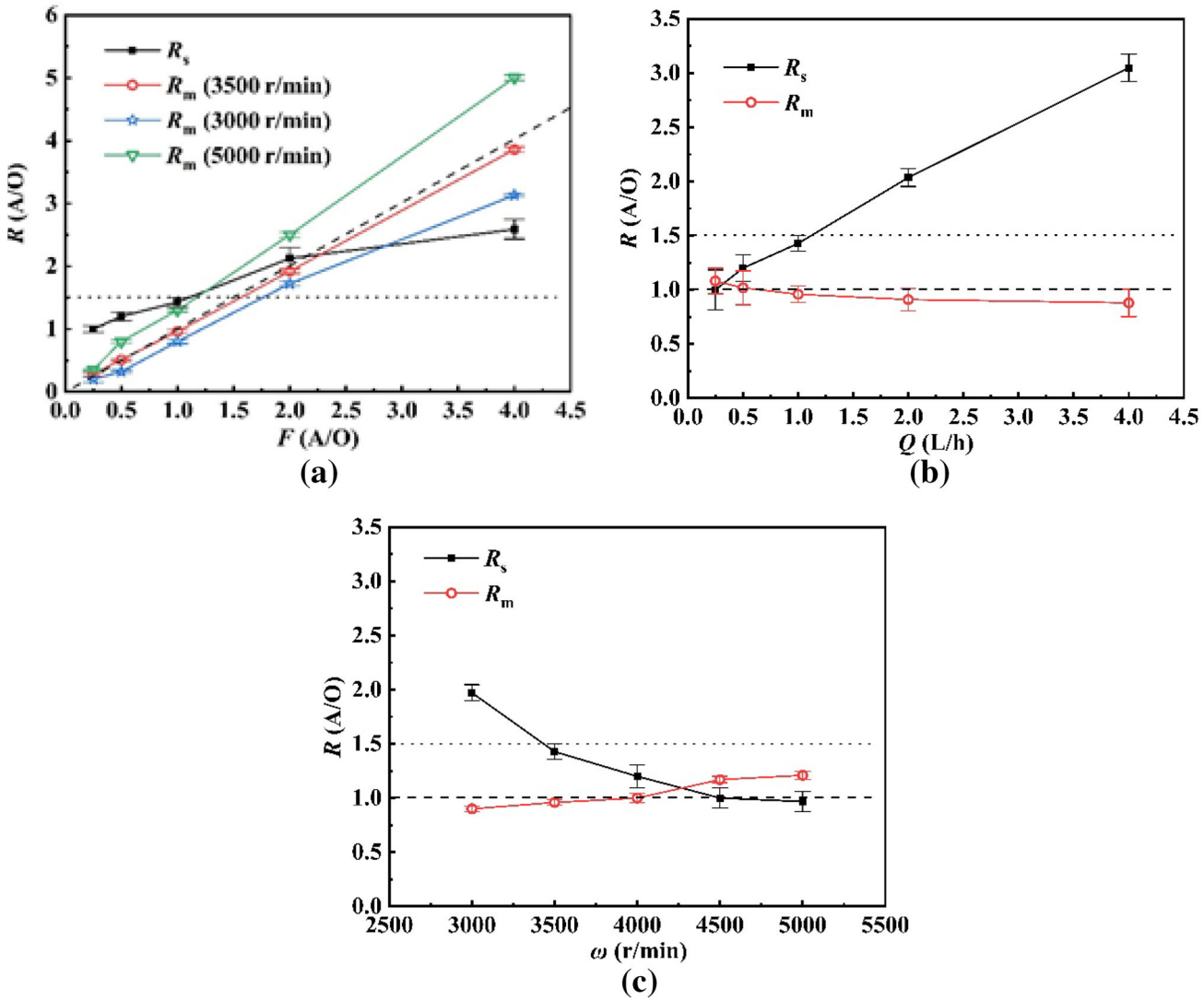

Fig. 9 Effects of the operational parameters on R (A/O). Dashed lines indicate F (A/O), solid lines indicate R_s (A/O) = 1.5 for the case where the interface position between the two phases in the separating zone was in the middle of the inner wall of the underflow and the light-phase weir

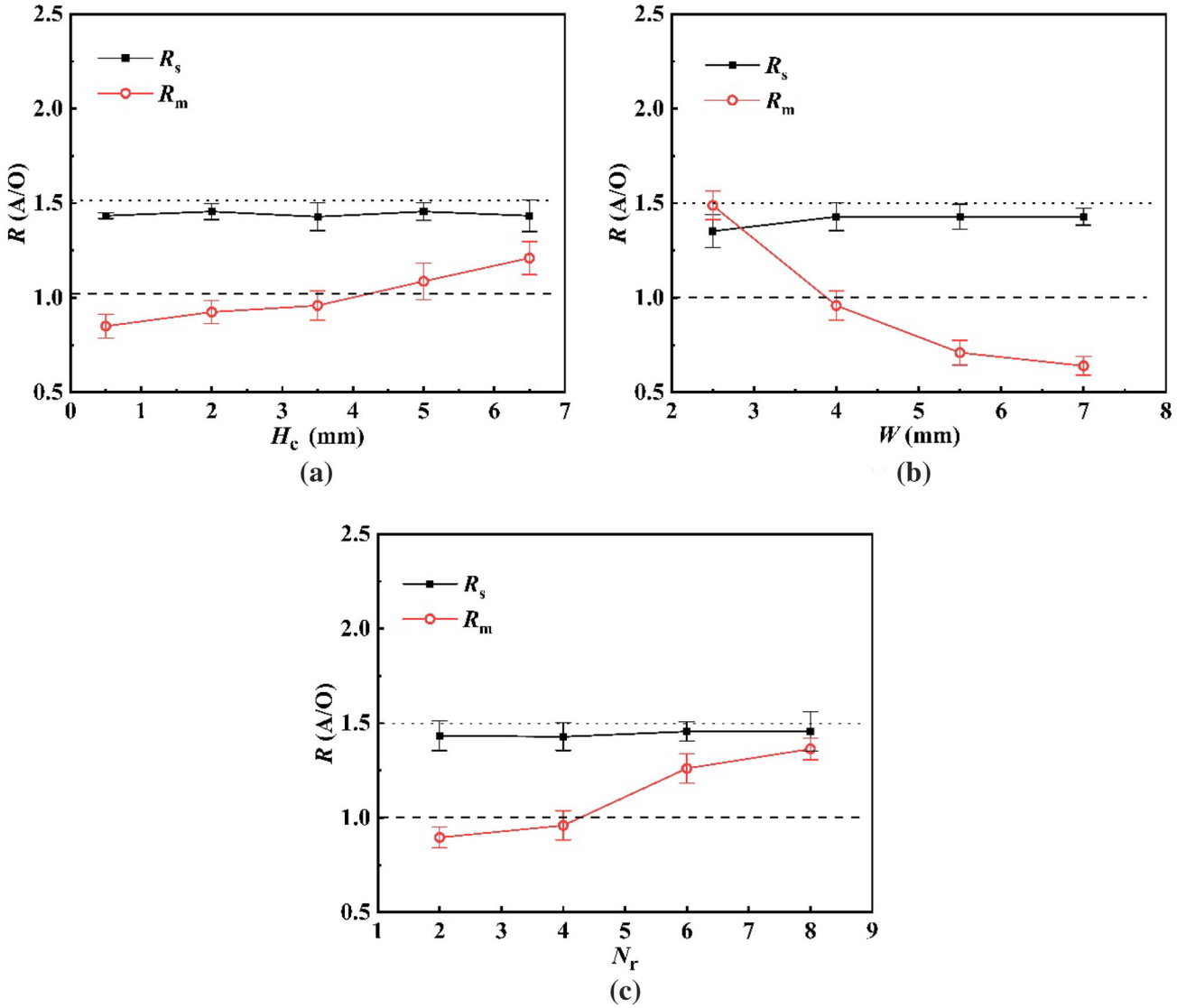

Fig. 10 Effects of the structural parameters of the housing on R (A/O). Dashed lines indicate F (A/O), solid lines indicate R_s (A/O) = 1.5 for the case where the interface position between the two phases in the separating zone was in the middle of the inner wall of the underflow and the light-phase weir

mixing zone were organic- and aqueous-rich regions, respectively. Via computational fluid dynamics simulations and experiments, Wardle showed that the center region between the radial vanes at the bottom of the housing contained an aqueous-rich region [28]. When ω was low and Q was large, V_m was large, as shown in Fig. 6; therefore, the organic-rich region accounted for the majority of the fluids in the mixing zone; accordingly, R_m (A/O) was lower than F (A/O). When ω was high or Q was small, V_m was small, as shown in Fig. 6. Thus, the aqueous-rich region accounted for the majority of the fluids in the mixing zone, and R_m (A/O) was higher than F (A/O).

In the ACC, the interface radius (r_i) of the two phases in the separating zone (Fig. 1) is determined as follows [13]:

$$r_i = r_A \sqrt{\frac{1 - \frac{\rho_O r_O^2}{\rho_A r_A^2}}{1 - \frac{\rho_O}{\rho_A}}}, \tag{3}$$

where r_i is the interface radius (mm), ρ_O is the density of the light phase (kg/m^3), ρ_A is the density of the heavy phase (kg/m^3), r_O is the actual liquid radius at the light-phase weir (mm), and r_A is the actual liquid radius at the heavy-phase weir (mm). However, determining r_i using Eq. (3) is difficult because both r_A and r_O are challenging to obtain. However, Eq. (3) can be used to analyze r_i qualitatively.

Zhao [21] and Duan and Cao [24] qualitatively analyzed the effects of the operational parameters on r_i by using Eq. (3). The results showed that r_i decreased with the

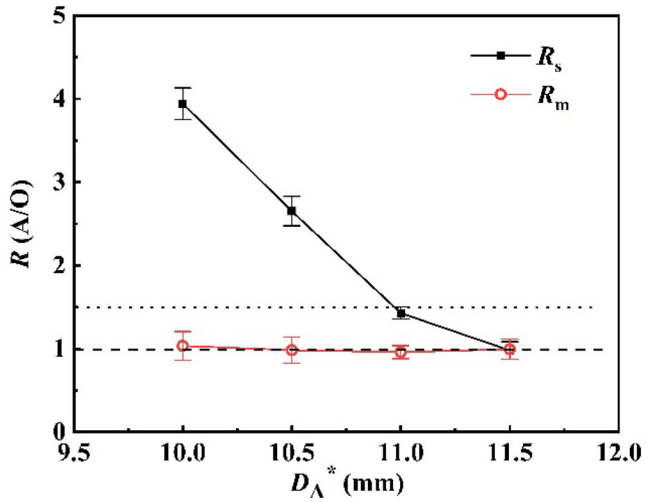
R_s
R_m
R (A/O)
D_A^* (mm)

(a)

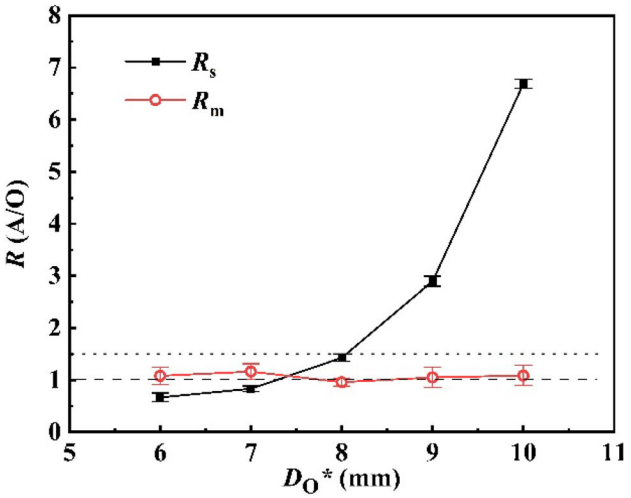
R_s
R_m
R (A/O)
D_O^* (mm)

(b)

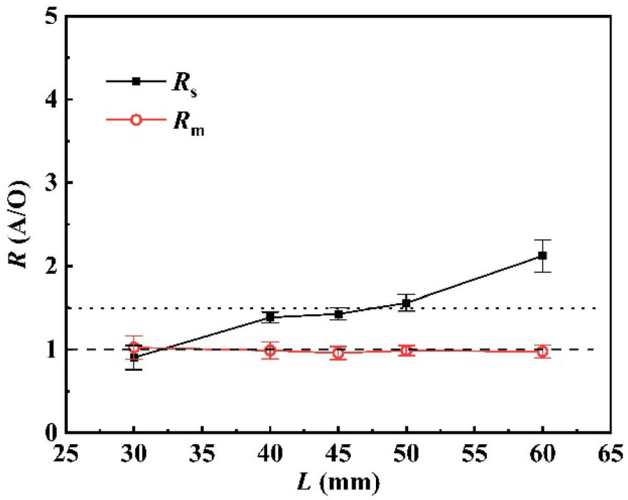
R_s
R_m
R (A/O)
L (mm)

(c)

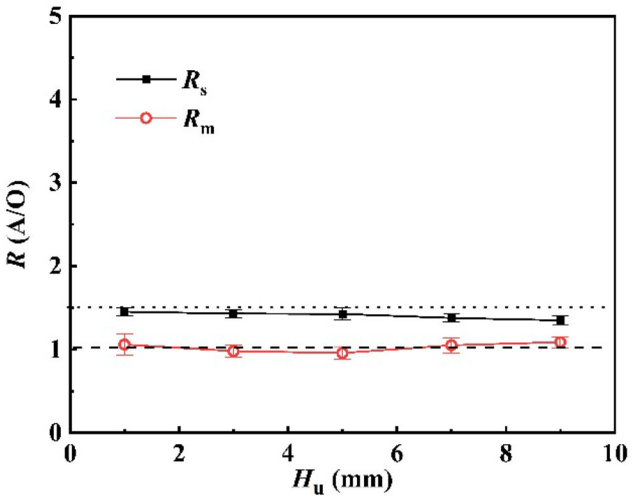
R_s
R_m
R (A/O)
H_u (mm)

(d)

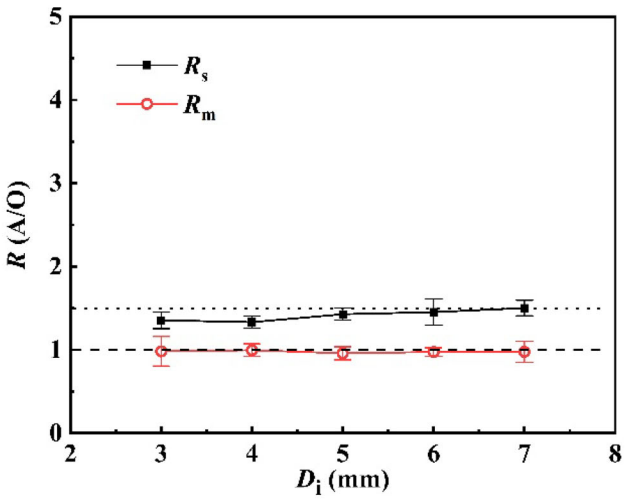
R_s
R_m
R (A/O)
D_i (mm)

(e)

◀**Fig. 11** Effects of the structural parameters of the rotor on R (A/O). Dashed lines indicate F (A/O), solid lines indicate R_s (A/O) = 1.5 for the case where the interface position between the two phases in the separating zone was in the middle of the inner wall of the underflow and the light-phase weir

increase in F (A/O) and Q and increased with the increase in ω, which was verified experimentally. The changes in R_s (A/O) are the same as the changes in r_i with the changes in F (A/O), Q, and ω. When R_s (A/O) is 1.5, the interface position between the two phases in the separating zone is in the middle of the inner wall of the underflow and the light-phase weir. A higher R_s (A/O) yields easier aqueous-phase entrainment in the organic-phase outlet, and a lower R_s (A/O) yields easier organic-phase entrainment in the aqueous-phase outlet.

3.3.2 Effects of structural parameters of housing

Figure 10 shows the effects of the structural parameters of the housing—H_c, W, and N_r—on R (A/O). R_s (A/O) hardly changed with respect to the structural parameters of the housing, because these parameters hardly affected the flow in the separating zone. R_m (A/O) decreased with the increase in W and increased with the increase in H_c and N_r. Moreover, R_m (A/O) was inconsistent with F (A/O). This is mainly because the organic- and aqueous-rich regions appeared in the upper and lower sections of the mixing zone, respectively. V_m increased with W, as shown in Fig. 7. Hence, R_m (A/O) decreased with the increase in W. When H_c increased, the liquids of the organic-rich region in the upper section of the mixing zone were initially absorbed in the rotor. The aqueous-rich region accounted for the majority of the fluids in the mixing zone. Thus, R_m (A/O) increased with H_c. When N_r increased, although V_m (and the ALH) increased, the aqueous-rich region also increased, because of the increase in the number of chambers between the radial vanes. Moreover, the aqueous-rich region accounted for the majority of the fluids in the mixing zone. Thus, R_m (A/O) increased with N_r.

3.3.3 Effects of structural parameters of rotor

Figure 11 shows the effects of the structural parameters of the rotor—D_A*, D_O*, L, H_u, and D_i—on R (A/O). R_m (A/O) hardly changed with respect to the structural parameters of the rotor and was nearly equal to F (A/O), because the parameters of the rotor hardly affected the flow in the mixing zone. R_s (A/O) increased with D_O* and L but decreased with the increase in D_A*, because r_i increased with D_A*. However, r_i decreased with the increase in D_O*, according to Eq. (3). According to the equations for r_A and r_O proposed in [29], with the increase in L, r_O increases, but r_A remains unchanged. Thus, in accordance with Eq. (3), r_i decreased, and R_s (A/O) increased. H_u and D_i hardly affected R_s (A/O), because they hardly influenced r_i according to Eq. (3).

The effects of N_a on R (A/O) are presented in Table 3. N_a hardly affected R_m (A/O), because it hardly influenced the geometric volume and flow of the mixing zone. R_s (A/O) decreased with the increase in N_a. According to the equations for r_A and r_O in [29], with the increase in N_a, r_O decreases, but r_A remains unchanged. Hence, in accordance with Eq. (3), r_i increased, and R_S (A/O) decreased.

4 Conclusion

For successfully designing and operating ACCs for RSNF, the effect of the HNO_3 concentration on N_{Di} for a 30%TBP/kerosene-HNO_3 solution system was investigated. Then, the effects of the operational and structural parameters on V and R (A/O) in both the mixing and separating zones of the ϕ20 ACC were systematically investigated using the liquid-fast-separation method and the 30%TBP/kerosene-HNO_3 solution system. The N_{Di} of the 30%TBP/kerosene-HNO_3 solution system was $> 14 \times 10^{-4}$; hence, the 30%TBP/kerosene-HNO_3 solution system should exhibit good phase-separation performance in the ACC. V_r hardly changed with respect to the operational parameters, the structural parameters of the housing, D_A*, and H_u but increased with L and N_r and decreased with the increase in D_O*. V_m hardly changed with respect to the structural parameters of the rotor but increased with F (A/O), Q, H_c, and W and decreased with the increase in ω and N_r. R_m (A/O) hardly changed with respect to the structural parameters of the rotor and N_a but decreased with the increase in Q and W and increased with ω, F (A/O), H_c, and N_r. R_s (A/O) hardly changed with respect to the structural parameters of the housing but decreased with the increase in ω, W, and D_A* and increased with Q, F (A/O), H_c, N_r, D_O*, L, and N_a. Additionally, R (A/O) was inconsistent with F (A/O), except in the case of suitable operational and structural parameters. These results are useful for understanding the flow characteristics and optimizing structure of ACCs.

References

1. S.T. Xiao, L. Li, G.A. Ye et al., An improvement in APOR process I-uranium/plutonium separation process. Nucl. Sci. Tech. **26**, 040605 (2015). https://doi.org/10.13538/j.1001-8042/nst.26.040605

2. R.A. Leonard, G.J. Bernstein, A.A. Ziegler et al., Annular centrifugal contactors for solvent extraction. Sep. Sci. Technol. **15**, 925–943 (1980). https://doi.org/10.1080/01496398008076278
3. R.A. Leonard, D.B. Chamberlain, C. Conner, Centrifugal contactors for laboratory-scale solvent extraction tests. Sep. Sci. Technol. **32**, 193–210 (1997). https://doi.org/10.1080/01496399708003194
4. W.H. Duan, T.X. Sun, J.C. Wang, An industrial-scale annular centrifugal extractor for the TRPO process. Nucl. Sci. Tech. **29**, 46 (2018). https://doi.org/10.1007/s41365-018-0395-z
5. W.H. Duan, M.M. Zhao, C.Q. Wang et al., Recent advances in the development and application of annular centrifugal contactors in the nuclear industry. Solvent Extr. Ion Exch. **32**, 1–26 (2014). https://doi.org/10.1080/07366299.2013.833741
6. R.J. Taylor, C.R. Gregson, M.J. Carrott et al., Progress towards the full recovery of neptunium in an advanced PUREX process. Solvent Extr. Ion Exch. **31**, 442–462 (2013). https://doi.org/10.1080/07366299.2013.800438
7. T.S. Rudisill, M.C. Thompson, Demonstration of the use of formohydroxamic acid in the UREX process. Sep. Sci. Technol. **50**, 2823–2831 (2015). https://doi.org/10.1080/01496395.2015.1085413
8. M. Carrott, K. Bell, J. Brown et al., Development of a new flowsheet for co-separating the transuranic actinides: the "EURO-GANEX" process. Solvent Extr. Ion Exch. **32**, 447–467 (2014). https://doi.org/10.1080/07366299.2014.896580
9. J.D. Law, T.G. Garn, D.H. Meikrantz et al., Pilot-scale TRUEX flowsheet testing for separation of actinides and lanthanides from used nuclear fuel. Sep. Sci. Technol. **45**, 1769–1775 (2010). https://doi.org/10.1080/01496395.2010.493832
10. R. Malmbeck, O. Courson, G. Pagliosa et al., Partitioning of minor actinides from HLLW using the DIAMEX process. Part 2-''hot'' continuous counter-current experiment. Radiochim. Acta **88**, 865–871 (2000). https://doi.org/10.1524/ract.2000.88.12.865
11. G. Modolo, H. Asp, H. Vijgen et al., Demonstration of a TODGA-based continuous counter-current extraction process for the partitioning of actinides from a simulated PUREX raffinate, part II: centrifugal contactor runs. Solvent Extr. Ion Exch. **26**, 62–76 (2008). https://doi.org/10.1080/07366290701784175
12. Y. Morita, M. Kubota, J.P. Glatz et al., Actinide partitioning from HLW in a continuous DIDPA extraction process by means of centrifugal extractors. Solvent Extr. Ion Exch. **14**, 385–400 (1996). https://doi.org/10.1080/07366299608918346
13. X.M. He, Y.S. Yan, Q.R. Zhang et al., Recent advances of annular centrifugal extractor for hot test of nuclear waste partitioning process. Nucl. Sci. Tech. **9**(3), 157–162 (1998)
14. W.H. Duan, J. Chen, J.C. Wang et al., Application of annular centrifugal contactors in the hot test of the improved total partitioning process for high level liquid waste. J. Hazard Mater. **278**, 566–571 (2014). https://doi.org/10.1016/j.jhazmat.2014.06.049
15. D.H. Meikrantz, T.G. Garn, J.D. Law et al., A centrifugal contactor design to facilitate remote replacement. Nucl. Technol. **173**, 289–299 (2011). https://doi.org/10.13182/NT11-A11662
16. K. Mandal, S. Kumar, V. Vijayakumar et al., Hydrodynamic and mass transfer studies of 125 mm centrifugal extractor with 30% TBP/nitric acid system. Prog. Nucl. Energy **85**, 1–10 (2015). https://doi.org/10.1016/j.pnucene.2015.05.005
17. W.H. Duan, C.L. Song, Q.L. Wu et al., Development and performance of a new annular centrifugal contactor for semi-industrial scale. Sep. Sci. Technol. **40**, 1871–1883 (2005). https://doi.org/10.1081/SS-200064531
18. K.E. Wardle, Liquid–liquid mixing studies in annular centrifugal contactors comparing stationary mixing vane options. Solvent Extr. Ion Exch. **33**, 671–690 (2015). https://doi.org/10.1080/07366299.2015.1082835
19. S.W. Li, W.H. Duan, J. Chen et al., CFD simulation of gas–liquid–liquid three-phase flow in an annular centrifugal contactor. Ind. Eng. Chem. Res. **51**, 11245–11253 (2012). https://doi.org/10.1021/ie300821t
20. S. Vedantam, K.E. Wardle, T.V. Tamhane et al., CFD simulation of annular centrifugal extractors. Int. J. Chem. Eng. **2012**, 759397 (2012). https://doi.org/10.1155/2012/759397
21. B.R. Zhao, A study on the interface radius and hold-up in an annular centrifugal extractor, M.D Dissertation. (Tsinghua University, 1996). **(In Chinese)**
22. B. Schuur, G.N. Kraai, J.G.M. Winkelman et al., Hydrodynamic features of centrifugal contactor separators: experimental studies on liquid hold-up, residence time distribution, phase behavior and drop size distributions. Chem. Eng. Process. **55**, 8–19 (2012). https://doi.org/10.1016/j.cep.2012.02.008
23. S.V.N. Ayyappa, M. Balamurugan, S. Kumar et al., Mass transfer and hydrodynamic studies in a 50 mm diameter centrifugal extractor. Chem. Eng. Process. **105**, 30–37 (2016). https://doi.org/10.1016/j.cep.2016.04.005
24. W.H. Duan, S. Cao, Determination of the liquid hold-up volume and the interface radius of an annular centrifugal contactor using the liquid-fast-separation method. Chem. Eng. Commun. **203**, 548–556 (2016). https://doi.org/10.1080/00986445.2015.1048802
25. W.H. Duan, Q. Cheng, X.Z. Zhou et al., Development of a ϕ 20 mm annular centrifugal contactor for the hot test of the total TRPO process. Prog. Nucl. Energy **51**, 313–318 (2009). https://doi.org/10.1016/j.pnucene.2008.08.002
26. R.A. Leonard, Solvent characterization using the dispersion number. Sep. Sci. Technol. **30**(7–9), 1103–1122 (1995). https://doi.org/10.1080/01496399508010335
27. K.E. Wardle, T.R. Allen, M.H. Anderson, Experimental study of the hydraulic operation of an annular centrifugal contactor with various mixing vane geometries. AIChE J. **56**(8), 1960–1974 (2010). https://doi.org/10.1002/aic
28. K.E. Wardle, *Summary Report on liquid-liquid contactor scoping experiments and validation test case definition, ANL-LTR-CERT-12-001*. Argonne National Laboratory, USA (2012)
29. G.J. Bernstein, D.E. Grosvenor, J.F. Lenc et al., *Development and performance of a high-speed, long-rotor centrifugal contactor for application to reprocessing LMFBR Fuels*. ANL-7968. Argonne National Laboratory, USA (1973)